Computational Materials Science 54 (2012) 48–55

Contents lists available at SciVerse ScienceDirect

Computational Materials Science

journal homepage: www.elsevier.com/locate/commatsci

Computational approach using Johnson–Cook model on dual phase steel

Y. Prawoto [a,*], M. Fanone [b], S. Shahedi [a], M.S. Ismail [a], W.B. Wan Nik [c]

[a] Department of Applied Mechanics and Design, Faculty of Mechanical Engineering, University Technology Malaysia, 81310 UTM, Skudai, Johor, Malaysia
[b] Mubea Inc., 1555 Atlantic Boulevard, Auburn Hills, MI 48326-1501, USA
[c] Maritime Technology Department, University Malaysia Terengganu, 21030 Kuala Terengganu, Malaysia

ARTICLE INFO

Article history:
Received 23 September 2011
Received in revised form 11 October 2011
Accepted 20 October 2011
Available online 11 December 2011

Keywords:
Dual phase
Johnson Cook
Heat treatment
Intercritical temperature
Steel
Abaqus

ABSTRACT

In this research, two different hypo-eutectoid steels with different carbon content and alloying elements were made into samples with dual phase ferrite martensite microstructure. Their morphology and the mechanical properties were then compared. Computational model varying the ferrite percentage was also proposed. The model adopts the failure rule of Johnson–Cook's. The result shows that the difference in mechanical property was not only due to the variation of the ferrite parts in them but also due to the shapes of the constituents. It tends to follow the continuum mechanics rule. It is also concluded that modeling using two-dimensional approach is sufficient to estimate the properties of the dual phase structure.

1. Introduction

This paper is related to previously published papers [1–3]. The detailed discussion on the fracture mechanics approach has been discussed in there. Hence, in this paper such discussion is omitted. The dual phase ferrite–martensite steels (DPS) have been used and gained importance as structural steels and automotive parts due to an outstanding combination of their high strength and excellent formability. DPS is characterized by having microstructures of fine-grained, polygonal ferrite with grains of martensite dispersed therein as the matrix. The strength of such steels is determined mainly by the volume fraction of martensite; whereas the ductility is determined by the volume fraction of the polygonal ferrite. Plenty of researchers have proved their beneficial characteristics ranging from static to dynamic properties (e.g. [1,4]). The authors have also proved that the strengthening is different from that of rule of mixture. The shape and the arrangement of the polygonal ferrite contribute to the DPS strength [4]. From the manufacturing point view, one of the most interesting observations is that varying its martensite or ferrite volume fractions can alter the mechanical properties of DPS. Furthermore, since the DPS steel consists of basically two constituents, polygonal ferrite and martensite matrix, its final properties also depend upon those constituents.

While the investigation on the effect of the ferrite volume fraction is done extensively, the investigation of materials that have the same volume fraction but varying the carbon content is not getting much attention. Similarly, while the influence of the alloying elements in conventional microstructures are quite understood, their influence on the DPS is also not getting much attention. This research mainly focuses on the effect of carbon content and alloying element on DPS. To accommodate this goal, two different hypo-eutectoid steels, AISI 1050 and AISI 4130H, were made into dual phase ferrite–martensite microstructure. Their morphology and mechanical properties were then compared. Subsequently, their mechanical properties were analyzed. Computational model varying the ferrite percentage was also made. Simply using the available data both for ferrite and martensite, the model incorporates the influence of the alloying element. The results seem to be in good agreement with the experimental results.

2. Experimental method

2.1. Material

Two different steels were selected for this purpose. For both types, the original shape of the samples was rod with the diameter of an inch. This size was selected due to its common size for application that is common in automotive parts, such as suspension parts, or other rotating parts that require resisting fatigue [5]. The steels had a chemical composition (wt.%) as given in Table 1. The accompanying mill sheet affirms the specification of AISI-SAE 1050, and 4130H. The chemical composition of which is also given

* Corresponding author. Tel.: +60 167 279048; fax: +60 755 6615.
E-mail address: yunan.prawoto@gmail.com (Y. Prawoto).

0927-0256/$ - see front matter © 2011 Elsevier B.V. All rights reserved.
doi:10.1016/j.commatsci.2011.10.021

Table 1
Chemical composition analysis results (wt.%).

Sample	C	Cr	Mn	P	S	Si	Mo
A	0.489	0.0	0.825	0.0090	0.0016	0.16	0.0
B	0.323	1.232	0.926	0.0097	0.0017	0.09	0.20
AISI spec. of 1050	0.48–0.53	n/a	0.60–0.90	0.04 Max.	0.05 Max.	n/a	n/a
AISI spec. of 4130H	0.28–0.33	0.40–0.60	0.30–0.70	0.035 Max.	0.040 Max.	0.15–0.30	0.15–0.25

Table 2
Temperature of intercritical annealing.

Samples (A: 1050)	Temp. (°C)	Hardness (HV)	Samples (B:4130H)	Temp. (°C)	Hardness (HV)
A as is	Below AC_1	194.1	B as is	Below AC_1	262.1
A1	750	397.9	B1	785	352.8
A2	770	404.9	B2	800	386.1
A3	785	436.9	B3	815	457.6
A4	840	474.9	B4	830	472.1
A5	Above AC_3	485.0	B5	Above AC_3	480.9
Tempered	AC_3	340.1	Tempered	AC_3	332.7

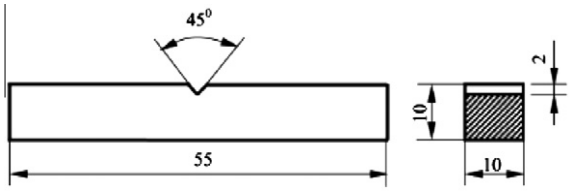

Fig. 1. Charpy impact test specimen used (unit in mm).

in the table. The composition is obtained by means of GDS (glow discharge spectroscopy) analysis.

2.2. Sample preparation

Following ASTM standards [6–8], the samples were machined using milling, wire cut and EDM (electrical discharge machining). Subsequently, the samples underwent intercritical heat treatment to produce dual phase steels. The samples were heated up to the area in between AC_1 and AC_3 temperatures and held for approximately 1 h. Table 2 shows the temperatures at which the samples were produced. Also shown in the table are the hardness values. On all samples, metallographic evaluation was performed mainly to estimate the ferrite percentage as well as to study their polygonal ferrite shape for computer modeling.

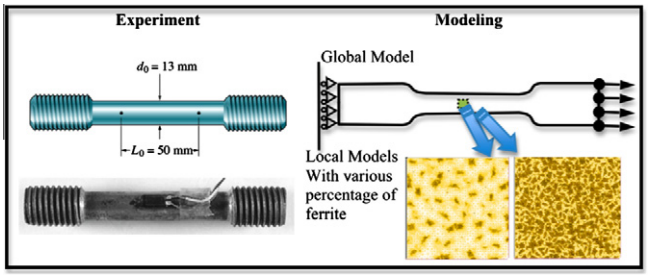

Fig. 2. Sub-modeling of the dual phase steel for tension analysis.

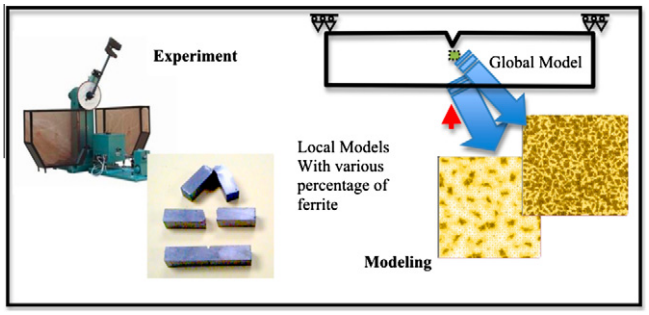

Fig. 3. Sub-modeling of the dual phase steel for impact analysis.

2.3. Mechanical test

Tensile and Charpy impact tests were performed on all samples. Fig. 1 shows the dimension of the samples used for the Charpy test. In general they are chosen because they are widely used in industry. Tensile test was chosen due to its basic characterization as well as to obtain parts of the constants for computational modeling purpose. The Charpy test was chosen because it is easy to prepare and to conduct and its results can be obtained quickly and cheaply. Even though the results are only comparative, it is still capable to

Table 3
Compilation of the Johnson Cook's material parameters for steel/metal.

Material/researcher	A	B	n	m	C	$\dot{\varepsilon}_0$
Ti6Al4V alloy, Dorogoy and Rittel [16]	880	695	0.36	0.8	0.04	1
Ti6Al4V alloy, Seo et al. [17]	998	653	0.45	0.7	0.0198	1
Ti, Meyer and Kleponis [18]	896	656	0.50	0.8	0.0128	1
Ti, Meyer and Kleponis [18]	863	331	0.34	0.8	0.0120	1
42CrMo, Lee and Lin [19]	724	683	0.47	1.0	0.035	10^{-5}
Weldox 460 E, Dey et al. [20]	499	382	0.458	0.893	0.0079	1
Weldox 460 E, Dey et al. [20]	859	329	0.579	1.071	0.0115	1
Weldox 460 E, Dey et al. [20]	992	364	0.568	1.131	0.0087	1
Ni-based superalloy steel, DeMange [21]	1138	1324	0.5	1.27	0.0092	1
Nitronic 33, Milani [22]	455	2289	0.834	0.258	0.066	1
AISI1006 steel, Wang [23]	350	275	0.36	1	0.022	1
AISI4340 steel, Wang [23]	792	509	0.26	1	0.014	1
S7 tool steel Wang [23]	1539	476	0.18	1	0.012	1
304 Stainless steel, Dean [24]	310	1000	0.65	1	0.07	0.01

determine the amount of energy absorbed by a material during fracture. This absorbed energy is a measure of a given material's toughness. In this research the speed used for tensile test was 10 mm/min and the energy used for Charpy impact test was 50 J. The difference between the initial and final potential energies was defined as the energy required to breaking the specimen.

3. Computational method

The computational method used in here is the same method discussed elsewhere [1–3]. While for the detailed method, the reader is advised to refer directly to the previous references; here very brief introduction of it is presented for the sake of reader's convenience. A commercial software *Abaqus*™ was used for modeling of simple tension test as well as the toughness computation.

In the modeling of the impact test, several choices that suitable to for *flow stress models* are available. Among them are:

- Johnson–Cook model [9].
- Zerilli–Armstrong model [10].
- Steinberg–Cochran–Guinan–Lund model [11].
- Mechanical Threshold Stress model [12].
- Preston–Tonks–Wallace model [13].

Table 4
Basic properties for model generation.

Mechanical properties (*Johnson Cook coeffs*)	Homogeneous (global model)		Dual phase (local model)			
	Sample A	Sample B	Sample A		Sample B	
			Ferrite	Martensite	Ferrite	Martensite
E (GPa)	185.5	185.5	124.7	200.1	124.7	200.1
α (MPa)	580	997	360	680	560	1140
B (MPa)	825	1231	545	913	812	1420
n	0.641	0.496	0.701	0.463	0.662	0.412
m	0.076	0.017	0.091	0.015	0.083	0.012
Poisson's ratio = 0.3125, m = 1						

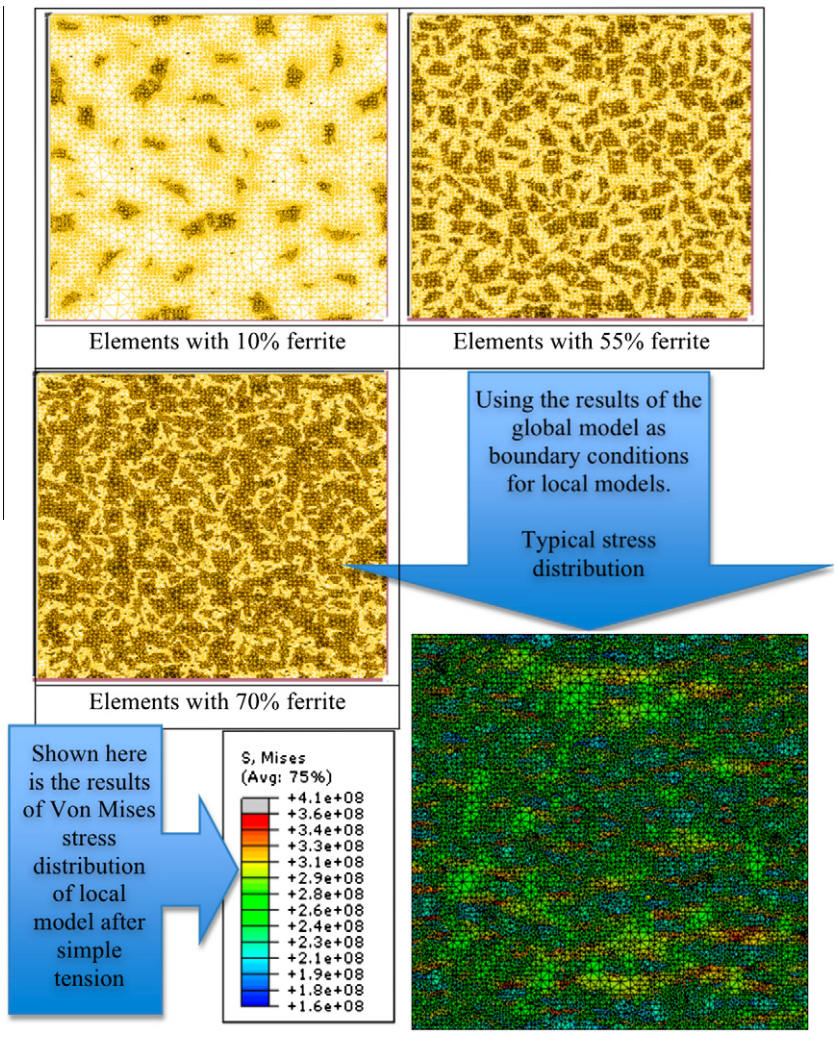

Fig. 4. Element of the local models and representative of stress distribution (tensile test).

These models are far more advanced and popular in the computational mechanics than the traditional pure theoretical models such as Von Mises model in terms of their capabilities in accommodating the evolution of the yield strength with respect to stress and strain rate. The Zerilli–Armstrong model is a simple physically based model that has been used extensively it is proven to work for tantalum and copper nicely [14]. A more complex model that is based on ideas from dislocation dynamics is the Mechanical Threshold Stress model. This model has been used to model the plastic deformation of some alloys of steel [15]. The Steinberg–Cochran–Guinan–Lund model is semi-empirical at low strain rate and purely empirical at high strain-rates. The Preston–Tonks–Wallace model is also physically based and has a form similar to the Mechanical Threshold Stress model. The Johnson–Cook model [9] is purely empirical and is the most widely used of the five, although this model exhibits only small strain-rate dependant at high temperatures. The fact that is being widely used carries the positive consequences, which are their constants are widely available. Further discussion on this is beyond the coverage of this paper, since this paper focus on the ferrite polygonal shape effect.

In here, the Johnson Cook [9] material model was employed to model the flow stress behavior of the material. In the Johnson–Cook model, as detailed in Eq. (1), the flow stress is expressed as a function of the strain ε, strain hardening index n, strain rate $\dot{\varepsilon}$, reference strain rate $\dot{\varepsilon}_0$, dimensionless homologous temperature $\widehat{T}$, which is $(T - T_r)/(T_m - T_r)$, work piece temperature T, reference temperature T_r, melting temperature T_m and strain-rate sensitivity index m.

$$\sigma^0 = (A + B(\varepsilon^p)^n) \cdot \left(1 + C \cdot \ln\left(\frac{\dot{\bar{\varepsilon}}^{pl}}{\dot{\bar{\varepsilon}}_0}\right)\right) \cdot (1 - \widehat{T}^m) \tag{1}$$

The damage is computed by the following.

$$\omega = \sum \left(\frac{\Delta\bar{\varepsilon}^{pl}}{\bar{\varepsilon}_f^{pl}}\right) \tag{2}$$

where $\Delta\bar{\varepsilon}^{pl}$ is an increment of equivalent plastic strain. $\bar{\varepsilon}_f^{pl}$ is the failure strain. When p is pressure stress and q is Mises stress, $\bar{\varepsilon}_f^{pl}$ is of:

$$\bar{\varepsilon}_f^{pl} = \left[d_1 + d_2 \exp\left(d_3 \frac{p}{q}\right)\right] \cdot \left[1 + d_4 \ln\left(\frac{\dot{\bar{\varepsilon}}^{pl}}{\dot{\bar{\varepsilon}}_0}\right)\right] \cdot (1 + d_5\hat{\theta}) \tag{3}$$

Being formulated less than 25 years ago, the Johnson–Cook equation is not known among the materials scientists. Therefore, the values of them are not comprehensively available. They are avail- able for several materials. Some of them are displayed in Table 3 [16–24]. Many of them are not derived directly by means of experiment.

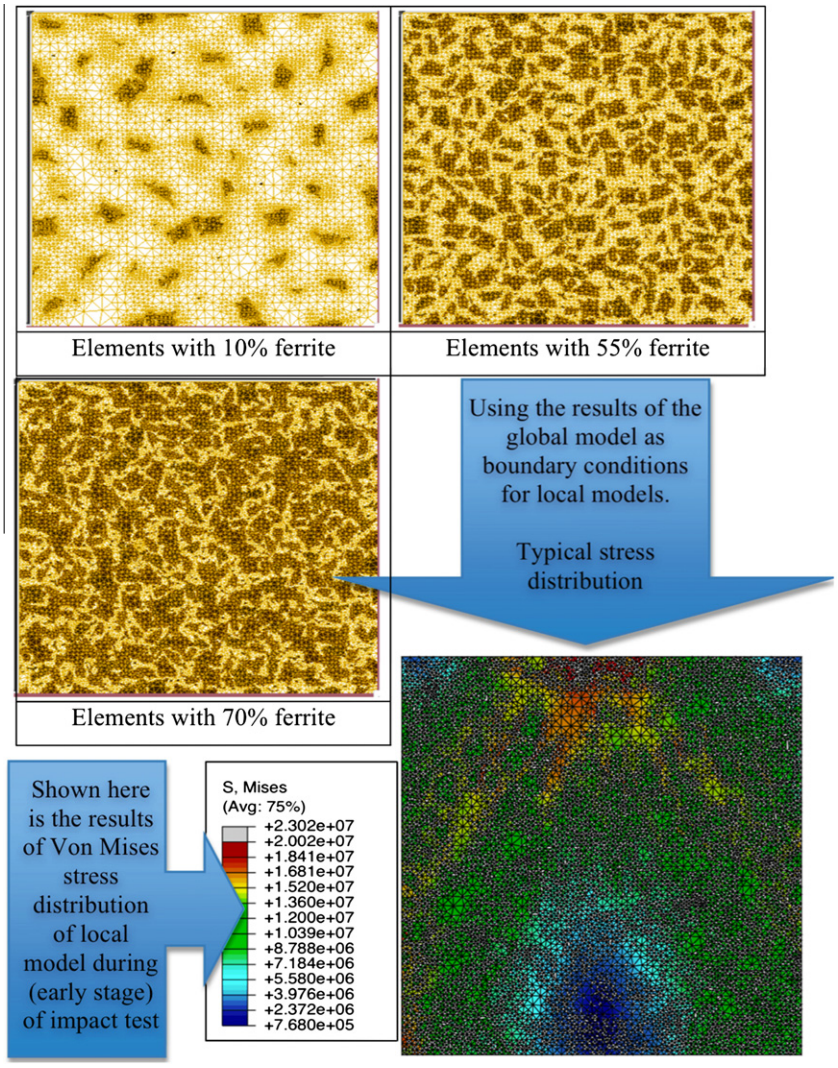

Fig. 5. Element of the local models and representative of stress distribution (impact).

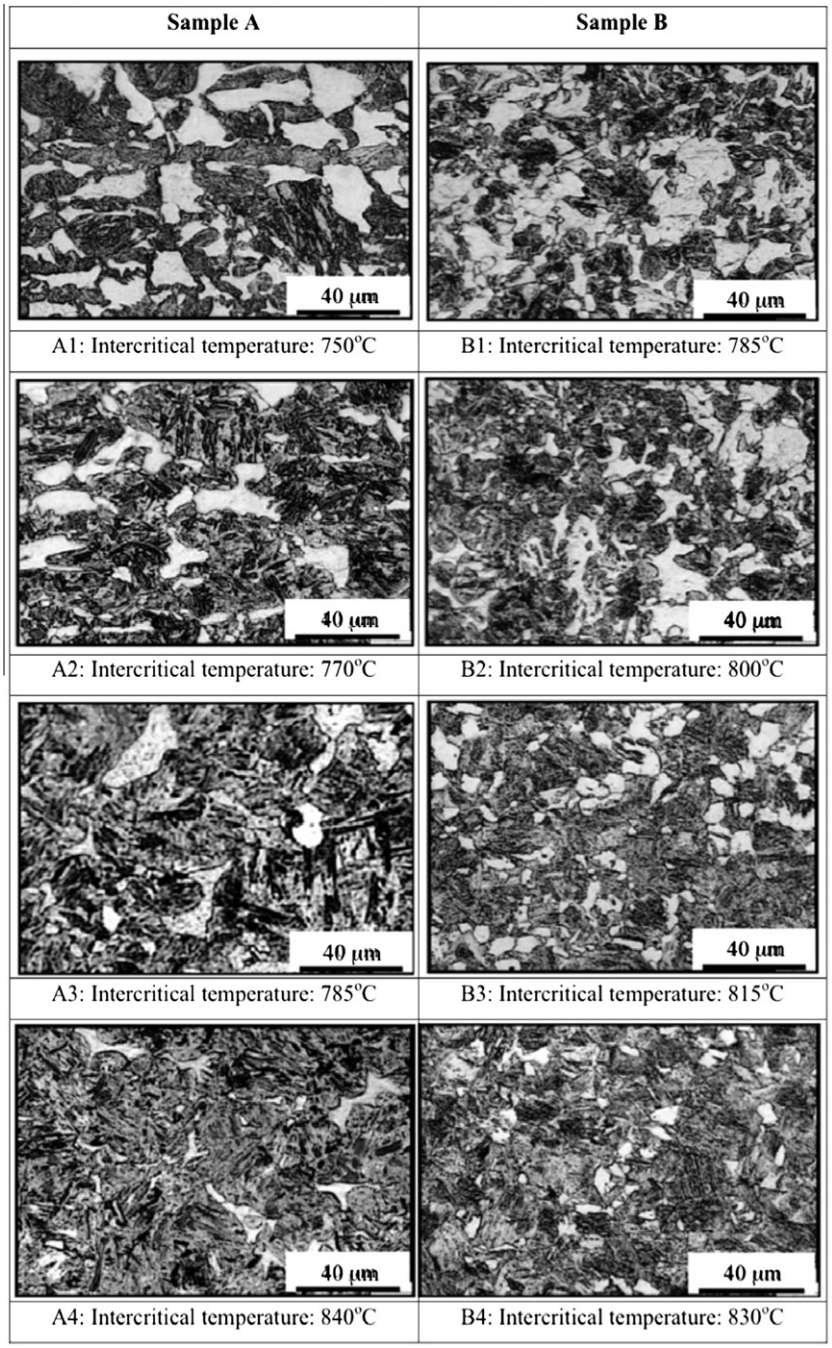

Fig. 6. Representative of the dual phase microstructures.

Table 5
Mechanical properties evaluation (mainly non-tempered samples).

Sample	Temp. (°C)	Micro-hardness (HV), avg of 5 measurements			UTS (MPa)	Impact energy (J)	
		Overall	α	α'		As quenched	Tempered
A1	750	397.9	160.4	491.6	806.7	8.0	27.3
A2	770	404.9	166.2	499.3	965.3	1.9	28.7
A3	785	436.9	164.7	500.4	1035.4	1.6	29.2
A4	840	474.9	165.5	505.8	1247.3	1.7	29.4
B1	785	352.8	206.3	526.4	706.7	14.6	20.7
B2	800	386.1	209.2	530.8	960.5	8.6	20.6
B3	815	457.6	231.4	531.6	1203.3	9.0	20.7
B4	830	472.1	242.5	523.5	1245.9	9.1	20.7

Note: α is ferrite and α' is martensite.

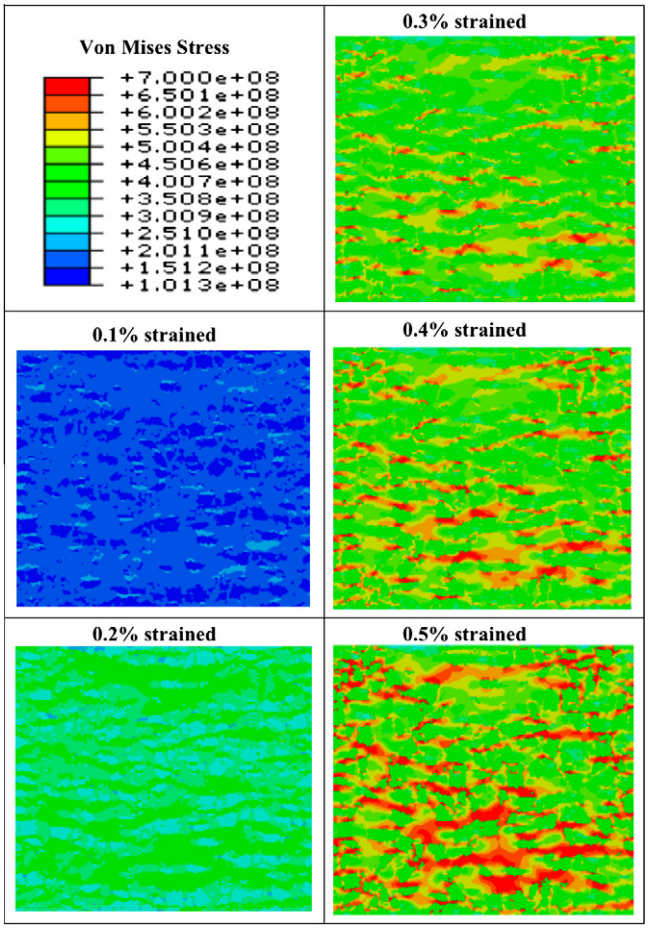

Fig. 7. Representative of the tensile test (40% α Fe and 60% α′ Fe).

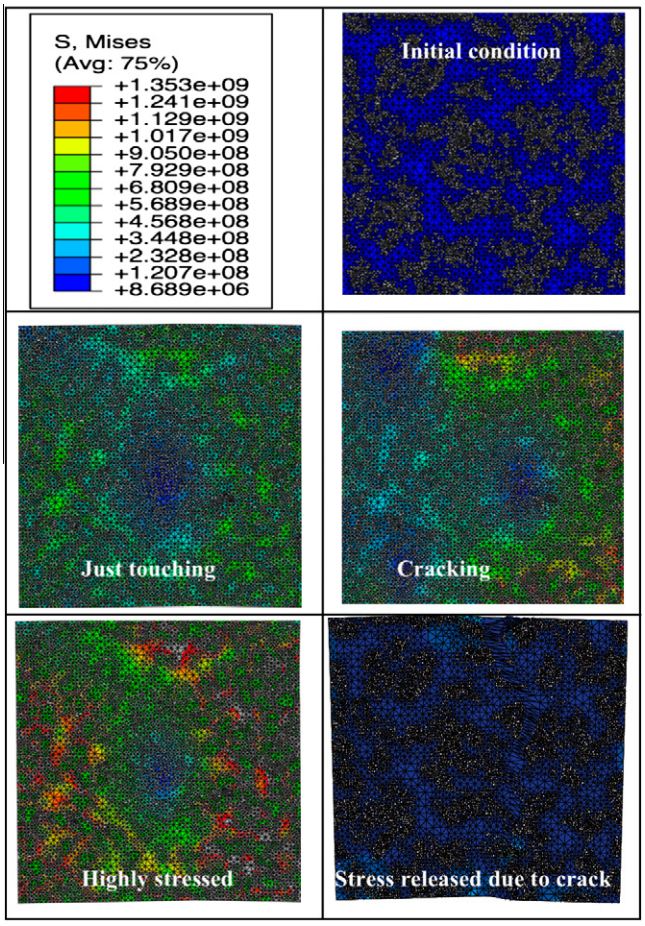

Fig. 9. Representative of the Charpy impact test (40% α Fe and 60% α′ Fe).

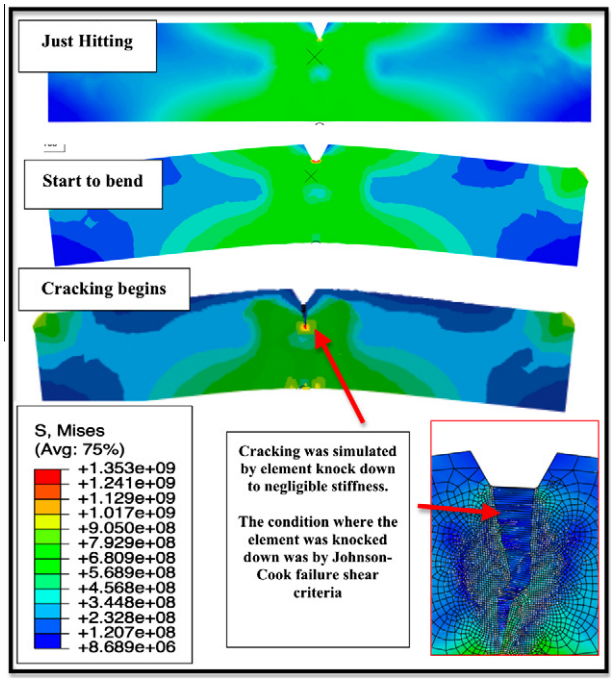

Fig. 8. Global model of the impact simulation using Johnson–Cook failure criterion.

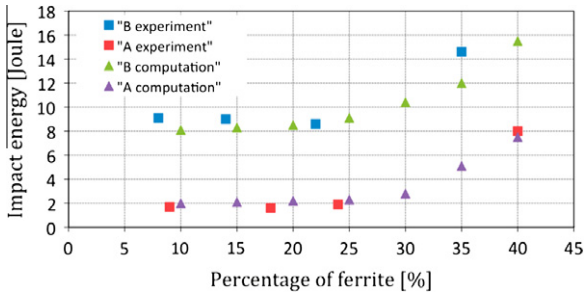

Fig. 10. Impact energy obtained both from experiment and computation.

Figs. 2 and 3 illustrate on how the sub-modeling concept is applied here both for static and dynamic evaluations. The element type used was CPE8 (8-node biquadratic element) and CPE6 (6-node quadratic element). Table 4 shows the basic values used for model creation. For the absorbed (impact) energy computation, Johnson and Cook model was used. The sub-modeling technique was used here. The sub-modeling technique allows the users to use the result of the global model as a boundary condition rather than giving the applied load. This technique allows the users to embed microstructure inside the model without the need to program in the form of multi-scale, which is cumbersome. Nor to model the whole structure with microstructure, which is practically almost impossible.

On these sub-models, basic properties shown in Table 4 were then applied. This table is used based on experimental tensile test and literature study. Therefore, the values are in no way accurate values. This is perfectly acceptable assumption since the value will

be normalized when it is compared with the experiment results. The important thing here is that the relative values follow the trend of the basic characteristics of each phase.

Instead of applying the applied force to the local models, the boundary conditions were applied to them. The boundary conditions are the one obtained from the computation results of the global model. Fig. 4 shows the element showing the element of the local model with the variation of ferrite constituent. It also shows the representative Von Mises stress distribution after load application. Due to the limited space, only one example is shown here. The models were created from 0% of ferrite up until 80% with the increment of 5%. Similar representative figure is shown in Fig. 5 for Charpy impact analysis.

4. Results and discussion

4.1. Morphology

Fig. 6 shows the representative of the dual phase of materials A and B. It shows that the percentage of polygonal ferrite reduces as the intercritical temperature increases. At similar temperature, the alloy steel has better polygonal ferrite distribution than that of carbon steel sample. Better distribution here means smaller size of colonies that are more evenly distributed and independent. Their diameters are typically less then 10 micron, while for the carbon steel sample the diameter could go double. Other researchers also agreed that alloying element has the capability of refining the grains for ferrous or non-ferrous alloys as well [25,26].

4.2. Mechanical properties

Mechanical property evaluation was done on all samples including microhardness on each constituent, tensile strength, and Charpy impact energy. Table 5 shows the summary of the results.

For the dual phase samples from medium carbon steel, the data obtained shows some fluctuations of the impact energy. It generally indicates that the energy absorbed decreases with increasing intercritical temperatures. In other words, higher volume percent of martensite formed in dual phase steel caused the impact toughness to reduce just as expected. Similar results have been reported [27]. These low toughness values indicate that without tempering, the dual phase samples are still very brittle even with the presence of considerable amounts of ferrite phase. One possible reason for this phenomenon may be related to the formation of massive amounts of dislocations accompanying the transformation of austenite to martensite. Since martensite (BCT) is lower in density compared to austenite (FCC), volume expansion during this transformation creates a strain field surrounding the polygonal ferrite. Such a strain field from martensite formation leads to a high dislocation content in the martensite itself. These high density dislocations will entangle to each other and hinder the dislocation motion as it was formed. Therefore, the dual phase steel ends up being brittle.

The opposite tendency was obtained from dual phase samples of alloy steel that shows an increase in the impact toughness with increasing intercritical temperatures. It follows the same trend obtained for hardness properties of these steel specimens. The increase is presumably due to tougher martensite formed at higher temperatures resulting from finer micro-constituents in the steel.

The decrease in the impact toughness has been attributed to the coarser ferrite obtained in the specimen with lower martensite content. Hence it can be concluded from the present investigation that higher toughness as well as hardness values are significantly associated with the finer distribution of martensite and ferrite composite microstructure. Bello et al. found similar results [28].

It is widely accepted that the strengthening mechanism in martensite is related to the density of the dislocation. The higher the density is, the harder the materials become. This fact is also seen and agreed by other researchers (e.g., [29]).

4.3. Computational modeling

Fig. 7 shows the representative results of the stress distribution as the sample is pulled with different loading. Figs. 8 and 9 show the same condition for impact loading. They show the stress distribution of DPS with 40%-ferrite 60%-martensite. In these figures, it is shown that due to the morphology of the ferrite that is not perfect circle, near the boundary of the ferrite–martensite the stress concentration occurs. Therefore, even if the load applied was within elastic limit, the stress was microscopically not linear. It is the same with that of composite. Therefore, from the mechanics point of view, DPS is composite material. Although other percentages of the modeling were also made and computed, here the picture presentation is omitted due to space limitation. The absorbed (impact) energy was estimated by the direct computation using the subroutine available on *Abaqus*™. The results are summarized in Fig. 10. In this figure, the value of the energy was normalized to compare with the experiment values.

The DPS simulated in two-dimensional modeling was able to catch up the trend in the energy needed to break the sample. Furthermore, the fact that the results do not agree with simple rule of mixture indicates that the impact energy is indeed different with other basic physical basic factor such as mass, or even Young's modulus. It is rather following the continuum mechanics principle, where the shape and geometry control the magnitude of the stress, which eventually determine if part of the constituents reach it's yielding.

Johson–Cook plasticity rule, together with the Johson–Cook failure criteria combined with the continuum mechanics approach was capable in describing and simulating the DPS failure quite accurately.

5. Conclusions

Two different hypo-eutectoid steels with different carbon content were made into dual phase ferrite martensite microstructure. The morphology and the mechanical properties of them were then compared. Subsequently, their mechanical properties were analyzed. The average size of the polygonal ferrite in DPS inherits its prior austenite grain size. Finer prior austenite grain size, due to alloying elements, produces also finer polygonal ferrite. Computational model varying the ferrite percentage was then made. The result shows that the mechanical property difference was due to the variation of martensitic parts of them. In contrast, the impact energy was highly influenced by the shape of the polygonal ferrite. It is also concluded that modeling using two-dimensional approach is sufficient to estimate the properties of the dual phase structure.

References

[1] Y. Prawoto, Mater. Sci. Eng., A 507 (2009) 74–86.
[2] Y. Prawoto, R. Idris, N. Kamsah, N. Tamin, Comput. Mater. Sci. 47 (2009) 482–490.
[3] Y. Prawoto, R. Idris, N. Kamsah, N. Tamin, Comput. Mater. Sci. 50 (2011) 1499–1503.
[4] L.R. Bhagavathi, Mater. Des. 32 (2011) 433–440.
[5] L. Zhonghua, H. Jiangbuo, W. Yonglan, K. Zenbang, Fatigue Fract. Eng. Mater. Struct. 13 (1990) 229–240.
[6] ASTM E8/E8M-09 Standard Test Methods for Tension Testing of Metallic Materials, ASTM International, West Conshohocken, PA, USA, 2009.

[7] ASTM A370-10 Standard Test Methods and Definitions for Mechanical Testing of Steel Products, ASTM International, West Conshohocken, PA, USA, 2010.
[8] ASTM E23-07 Standard Test Methods for Notched Bar Impact Testing of Metallic Materials, ASTM International, West Conshohocken, PA, USA, 2007.
[9] G.R. Johnson, W.H. Cook, Eng. Fract. Mech. 21 (1985) 31–48.
[10] F.J. Zerilli, R.W. Armstrong, J. Appl. Phys. 61 (1986) 1816–1825.
[11] D.J. Steinberg, S.G. Cochran, M.W. Guinan, J. Appl. Phys. 51 (1987) 1498–1504.
[12] P.S. Follansbee, U.F. Kocks, Acta Metall. 36 (1) (1988) 81–93.
[13] D.L. Preston, D.L. Tonks, D.C. Wallace, J. Appl. Phys. 93 (1) (2003) 211–220.
[14] R.W. Armstrong, F.J. Zerilli, J. Phys. D Appl. Phys. 43 (2010) 1–5.
[15] B. Banerjee, Int. J. Solids Struct. 44 (2007) 834–859.
[16] A. Dorogoy, D. Rittel, Exp. Mech. 49 (2009) 881–885.
[17] S. Seo, O. Min, H. Yang, Int. J. Impact Eng. 31 (2005) 735–754.
[18] H.W. Meyer, D.S. Kleponis, Int. J. Impact Eng. 26 (2001) 509–521.
[19] W.S. Lee, C.F. Lin, Mater. Sci. Eng., A 241 (1998) 48–59.
[20] S. Dey, T. Børvik, O.S. Hopperstad, M. Langseth, Comput. Mater. Sci. 38 (2006) 176–191.
[21] J.J. DeMange, Int. J. Impact Eng. 36 (2009) 1027–1043.
[22] A.S. Milani, Int. J. Impact Eng. 36 (2009) 294–302.
[23] X.B. Wang, Trans. Nonferrous Met. SOC China 16 (2006) 1362–1369.
[24] J. Dean, Compos. Struct. 93 (2011) 1089–1095.
[25] T. Engh, Principles of Metal Refining, Oxford University Press, New York USA, 1992.
[26] Y.C. Lee, A.K. Dahl, D.H. StJohn, Metall. Mater. Trans. 31 (11) (2000) 2895–2906.
[27] K. V Sudhakar, E.S. Dwarakadasa, Bulet. Mater. Sci. 23 (2000) 193–199.
[28] K.A. Bello, S.B. Hassan, M. Abdulwahab, U. Shehu, L.E. Umoru, A. Oyetunji, I.Y. Suleiman, J. Basic Appl. Sci. 1 (4) (2007) 407–414.
[29] J. Shi, S. Turteltaub, E. Van der Giessen, J. Mech. Phys. Solids 58 (11) (2010) 1863–1878.